OPEN

NPG Asia Materials (2015) 7, e171; doi:10.1038/am.2015.23

www.nature.com/am

ORIGINAL ARTICLE

$Cu/Li_4Ti_5O_{12}$ scaffolds as superior anodes for lithium-ion batteries

Xi Wang[1], Dequan Liu[1,2], Qunhong Weng[1], Jiangwei Liu[1], Qifeng Liang[3] and Chao Zhang[1]

Nanostructured active materials with both high-capacity and high-rate capability have attracted considerable attention, but they remain a great challenge to be realized. Herein, we report a new route to fabricate a bicontinuous $Cu/Li_4Ti_5O_{12}$ scaffold that consists of $Li_4Ti_5O_{12}$ nanoparticles (LTO NPs) with highly exposed (111) facets and nanoporous Cu scaffolds, which enable simultaneous high-capacity and high-rate lithium storage. It is a 'one stone, two birds' strategy. When tested as the anode in lithium-ion batteries LIBs, Cu/LTO showed superior performance, such as a lifespan greater than 2000 cycles and an ultrafast charging time (<45 s). Notably, the ultrahigh capacity slightly larger than the theoretical value was also observed in Cu/LTO at low current density. Density functional theory calculations and detailed characterizations revealed that the highly exposed (111) facets on the edge are the reason for its unique storage mechanism (8a+16c), which is different from the transition between 8a and 16c in bulk LTO.
NPG Asia Materials (2015) **7,** e171; doi:10.1038/am.2015.23; published online 10 April 2015

INTRODUCTION

It is well known that rechargeable batteries usually store considerably more energy than capacitors but deliver lower power.[1–3] To enhance ion and electron-transport kinetics in batteries, many approaches have been utilized, such as conductive layer coating, synthesis of the electrode material at the nanoscale and ion-doping.[4–6] Very recently, designing three-dimensional bicontinuous current collector/active material hybrid electrodes, which showed both high electron and ion conductivity,[7–9] has proven to be another facile and effective approach. In addition, NiOOH/nickel composite scaffold cathodes[7] and Au–Ge electrodes have been proposed.[8] Accompanied by the development of nanotechnology and science, nanostructured electrode materials with exposed highly reactive crystal planes (Figure 1a) can now demonstrate promising properties, including higher electrochemical performance.[10–13] A good example is the (111) facet of Co_3O_4 nanocrystals;[10] the (111) facet is desirable for LIBs and shows a larger capacity than the (001) plane. Another example is $Li_4Ti_5O_{12}$ films with (111) planes, which showed better ion transport properties and thus greater Li storage performance than samples with other planes exposed.[13] However, it remains a great challenge to concurrently obtain nanostructured active materials with both highly exposed planes and efficient ion and electron pathways.

Herein, we report a new route to fabricate a bicontinuous $Cu/Li_4Ti_5O_{12}$ scaffold electrode that consists of LTO NPs with highly exposed (111) facets and nanoporous Cu scaffold to enhance the electron and ion transport and thus enable high-capacity and high-rate lithium storage. LTO is chosen in this study because of its high Li insertion voltage (*ca.* 1.5 V vs Li^+/Li) and zero-strain insertion property, but its low electrical conductivity ($\sim 10^{-13}$ S cm^{-1}) and lithium diffusion coefficient ($\sim 10^{-13}$ cm^2 s^{-1}) hinder ultrafast lithium storage.[4,14,15] As illustrated in Figure 1a, in the commonly constructed LTO electrode architecture, there exist four primary resistances during the charging–discharging process: (1) Li^+ transport in the electrolyte; (2) Li^+ transfer from the electrolyte to the LTO electrode; (3) Li^+ diffusion in the electrode; and (4)electron conductance in the electrode and current collector. To realize the supercapacitor-like rate performance, a nanoporous Cu scaffold (NPCu) is used here as a template, and LTO NPs are then encapsulated into the nanopores of NPCu, as depicted in Figure 1c. It is a 'one stone, two birds' strategy. On one hand, the NPCu provides greater electroconductivity than the typical current collector and electrode structure. On the other hand, it is possible to obtain LTO NPs with their active planes highly exposed, which can provide high lithium ion conductivity in the unique Cu/LTO architecture. This result can be partly attributed to the strict space-confining effect within the nanosized pores of NPCu and the high proportion of curved surfaces present in the nanopores of the NPCu interior (Figure 1c).

[1]International Center for Young Scientists (ICYS), World Premier International (WPI) Center for Materials Nanoarchitectonics (MANA), National Institute for Materials Science (NIMS), Tsukuba, Ibaraki, Japan; [2]School of Physical Science and Technology, Lanzhou University, Lanzhou, People's Republic of China and [3]Department of Physics, Shaoxing University, Shaoxing, People's Republic of China
Correspondence: Dr X Wang, International Center for Young Scientists (ICYS), World Premier International (WPI) Center for Materials Nanoarchitectonics (MANA), National Institute for Materials Science (NIMS), Namiki 1-1, Tsukuba, Ibaraki 305-0044, Japan.
E-mail: wangxicas@gmail.com or wang.xi2@nims.go.jp
or Professor Q Liang, Department of Physics, Shaoxing University, Shaoxing 312000, People's Republic of China.
E-mail: qfliang@usx.edu.cn
Received 2 September 2014; revised 25 January 2015; accepted 15 February 2015

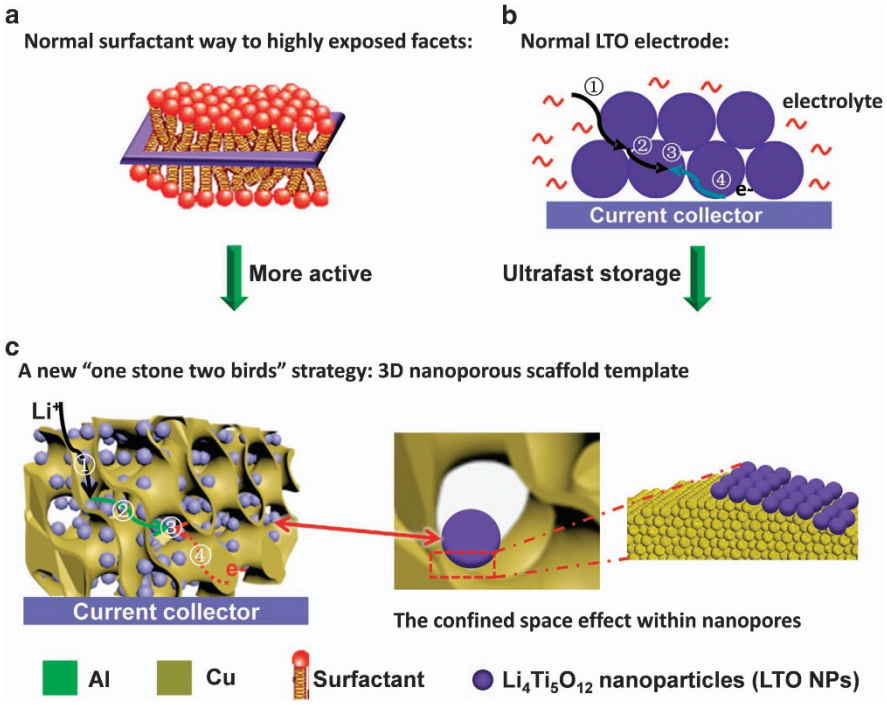

Figure 1 Comparison of two traditionally used methods and the new strategy of a Cu/LTO scaffold: (**a**) Illustration of the normal surfactant method to obtain nanomaterials with highly exposed planes. (**b**) Schematic representation of a commonly used electrode consisting of LTO particles, an electrolyte and a current collector. Four primary resistances are present in this electrode structure during the charging/discharging process: (1) ion transport in the electrolyte; (2) ion transport in the electrode; (3) electrochemical reactions in the electrode; and (4) electron conduction in the electrode and current collector. (**c**) Schematic illustration of a new 'one stone, two birds' strategy to fabricate a bicontinuous Cu/LTO electrode via a three-dimensional nanoporous Cu scaffold template route, where LTO NPs can be encapsulated into the Cu nanopores.

MATERIALS AND METHODS

Synthesis of nanoporous Cu/LTO scaffold

In the first step, nanoporous Cu scaffold templates (NPCu) were prepared. In the typical experiments, $Cu_{50}Al_{50}$ alloy ingots obtained by the electron-beam melting method were coated with a thin layer of Cu to avoid template collapse and were then selectively etched (Al) in aqueous NaOH solution until no hydrogen bubbles were observed. As-prepared NPCu foam was placed into 2.8 ml of solution containing 5 mM of $TiCl_4$ and 21 mg of $LiOH{\cdot}H_2O$. After storing in a dry and closed environment for approximately 1–5 h, the as-made product was washed with ethanol and water three times, dried at 100 °C for 6 h and finally calcined at 600 °C for 1.5 h in a mixed gas (5% v/v H_2 in Ar).

Characterization

JEOL 3000F and 2100F microscopes were used to observe the morphology of the final products, whereas a Hitachi S4800 electron microscope operating at 15 kV was utilized to obtain scanning electronic microscopy images. To record the X-ray diffraction patterns, a Philips X Pert PRO MPD X-ray diffractometer was utilized and operated at 35 kV and 45 mA with Cu Kα radiation. XPS measurements were carried out on an ESCALab220i-XL spectrometer by using a twin-anode Al Ka (1486.6 eV) X-ray source in which all the spectra were calibrated to the binding energy of the C 1-s peak at 284.6 eV.

Electrochemical test

A Hokudo Denko charge/discharge instrument was utilized to determine the electrochemical properties of the samples. The electrolyte was 1 M $LiClO_4$ in ethyl carbonate (EC) and diethyl carbonate (DEC; EC: DEC = 1:1 in v/v). The cells were assembled in a glove box filled with pure argon gas. Galvanostatic discharge/charge measurements were performed over a potential range of 2.5 V – 1 V vs Li^+/Li. Here the specific capacity of the Cu/LTO was calculated based on the weight of LTO.

Density functional theory calculations

All ground-state energies were calculated using the generalized gradient approximation to the density functional theory as implemented in the Vienna ab initio simulation package (VASP).

RESULTS AND DISCUSSION

Characterization of the Cu/LTO scaffold

Supplementary Figure S1 shows the fabrication process of the Cu/LTO electrode. Two steps are used here: the selective etching of Al from a Cu–Al alloy to obtain NPCu supports and the encapsulation of LTO NPs into the NPCu. The X-ray diffraction patterns of Cu/LTO (Supplementary Figure S2) are well indexed as spinel $Li_4Ti_5O_{12}$ (JCPDS Card No. 49–0207, space group $Fd\bar{3}m$ (227)) together with cubic Cu (JCPDS: 00004-0836, space group $Fm\bar{3}m$). In addition, a small rutile TiO_2 impurity (JCPDS Card No. 21–1276, marked as blue circle, Supplementary Figure S2) can be found in the final product. From Figures 2a,b and Supplementary Figure S3, one can observe that NPCu foam exhibits a bicontinuous structure consisting of nanopores with a pore size of ~50–100 nm. Another remarkable feature of NPCu is its ultrahigh electrical conductivity at room temperature. The inset schematic figure of NPCu in Figure 2 clearly shows its bicontinuous porosity.

After *in situ* growth and annealing treatment, the LTO NPs are well encapsulated into the interdigitated highly porous metallic scaffolds, leading to the formation of the bicontinuous Cu/LTO electrodes (Figure 2d). Consequently, the electron and ion transport lengths in the active material (LTO) and electrolyte can theoretically be shortened simultaneously, resulting in the high power density, and the active materials (LTO NPs) can be well filled in these three-dimensional nanoporous scaffolds compared with the traditional

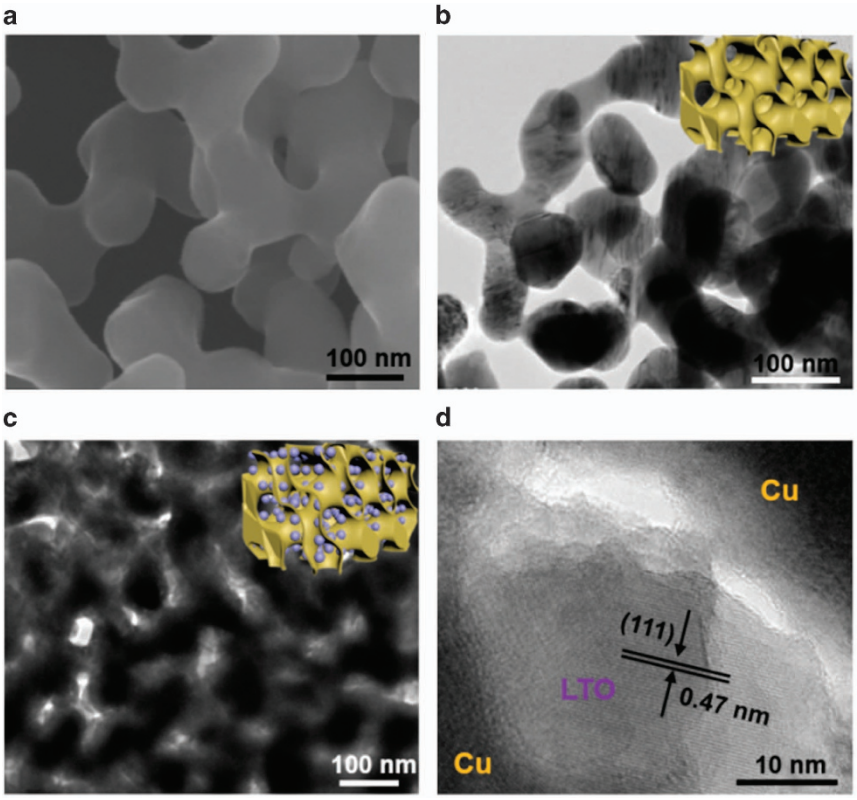

Figure 2 Structural analysis of a Cu/LTO scaffold anode: (**a**, **b**) scanning electronic microscopy and transmission electron microscopy (TEM) images of an as-made bicontinuous three-dimensional copper scaffold template after dealloying treatment. Inset shows the schematic representation of a piece of the Cu scaffold. (**c**, **d**) Low- and high-magnification TEM images of the Cu/LTO sample. Inset showing the schematic drawing of the Cu/LTO.

2D Cu foil templates, leading to the high energy density.[7–9] The size of the resulting LTO NPs varies from 30 to 90 nm, depending on the diameter of the NPCu's pores. Figure 2d shows the HRTEM image of a single LTO NP within Cu/LTO. The observed d-spacing of 0.47 nm matches well with that of the {111} facets of spinel $Li_4Ti_5O_{12}$. In addition, an epitaxial growth may exist in Cu/LTO systems based on density functional theory calculations (Supplementary Figure S4), in which Cu (111) has the lowest surface energy. This growth is similar to the epitaxial growth synthesis of LTO films with the same orientation on $SrTiO_3$ substrates, including LTO (111) on $SrTiO_3$ (111) and LTO (110) on $SrTiO_3$ (110).[13]

High rate capability and high capacity of Cu/LTO scaffold for lithium storage

The Cu/LTO was fabricated into coin cells to investigate its potential application in Li ion batteries.[14–23] As illustrated in Figure 3a, the as-made Cu/LTO not only can deliver ultrahigh capacity close to the theoretical value, but also possesses super cyclic capacity retention. For instance, after 1200 charge/discharge cycles, Cu/LTO can deliver an ultrahigh reversible capacity of 172 mAh g^{-1}, which is comparable to the theoretical value (175 mAh g^{-1}). Figure 3b shows the 1st, 50th, 100th, 600th and 1200th cycle discharge–charge voltage profiles for Cu/LTO at a current density of 0.5 C. The curves are characteristic of an LTO electrochemical pathway. The negligible change in the curve shape indicates that the present three-dimensional nanoporous architectures are indeed beneficial for the improvement of LTO anode materials. Although a small amount of rutile TiO_2 exists in the Cu/LTO, the typical plateaus of TiO_2 are not observed.[23] This result indicates that the contribution to the electrochemical performance of the whole electrode from the impurity is negligible. Note that under low current density (for example, 0.1 C), the capacity of Cu/LTO will exceed the theoretical value of 175 mAh g^{-1} and will exhibit very high stability in cyclic performance (Supplementary Figure S5). This phenomenon can usually be found in 10–30 nm sized LTO particles.[24]

More significantly, the Cu/LTO electrode exhibits ultrafast lithium storage properties, as shown in Figure 3c. For example, the Cu/LTO electrode can maintain a high capacity when the current density is increased to 5 C or 20 C. Notably, at a very high current rate of 80 C, corresponding to a charge time of ~45 s, the reversible capacity of Cu/LTO can still reach 127 mAh g^{-1}. These results are far superior to those of other anode materials,[14–22] which clearly demonstrates that Cu/LTO is a promising high-energy and high-power electrode material for LIBs. In addition, Cu/LTO exhibits high-rate cycling performance, maintaining ultrastable capacity at 1 C for over 2000 cycles (Figure 3d). The fast Li^+ transport of Cu/LTO is further observed from the small polarization for Cu/LTO (differences between the potentials of the charge plateaus and discharge plateaus).[5]

There are few reports of such a good performance at these high rates in the literature. The performance of the as-made Cu/LTO at such high rates is significantly better than that of other $Li_4Ti_5O_{12}$-based high-rate electrodes in recently reported works.[5,14–22] As shown in the compared results presented in Figure 3e, these reported electrodes include rutile TiO_2-coated LTO,[5] nanocrystalline LTO,[14] Zr-doped LTO,[15] carbon-coated LTO,[16] Cr-doped LTO,[17] LTO nanowire arrays,[18] mesoporous $Li_4Ti_5O_{12}$/C,[19] LTO nanotube arrays,[20] nanostructured LTO grown on rGO[21] and various doped LTO structures.[22]

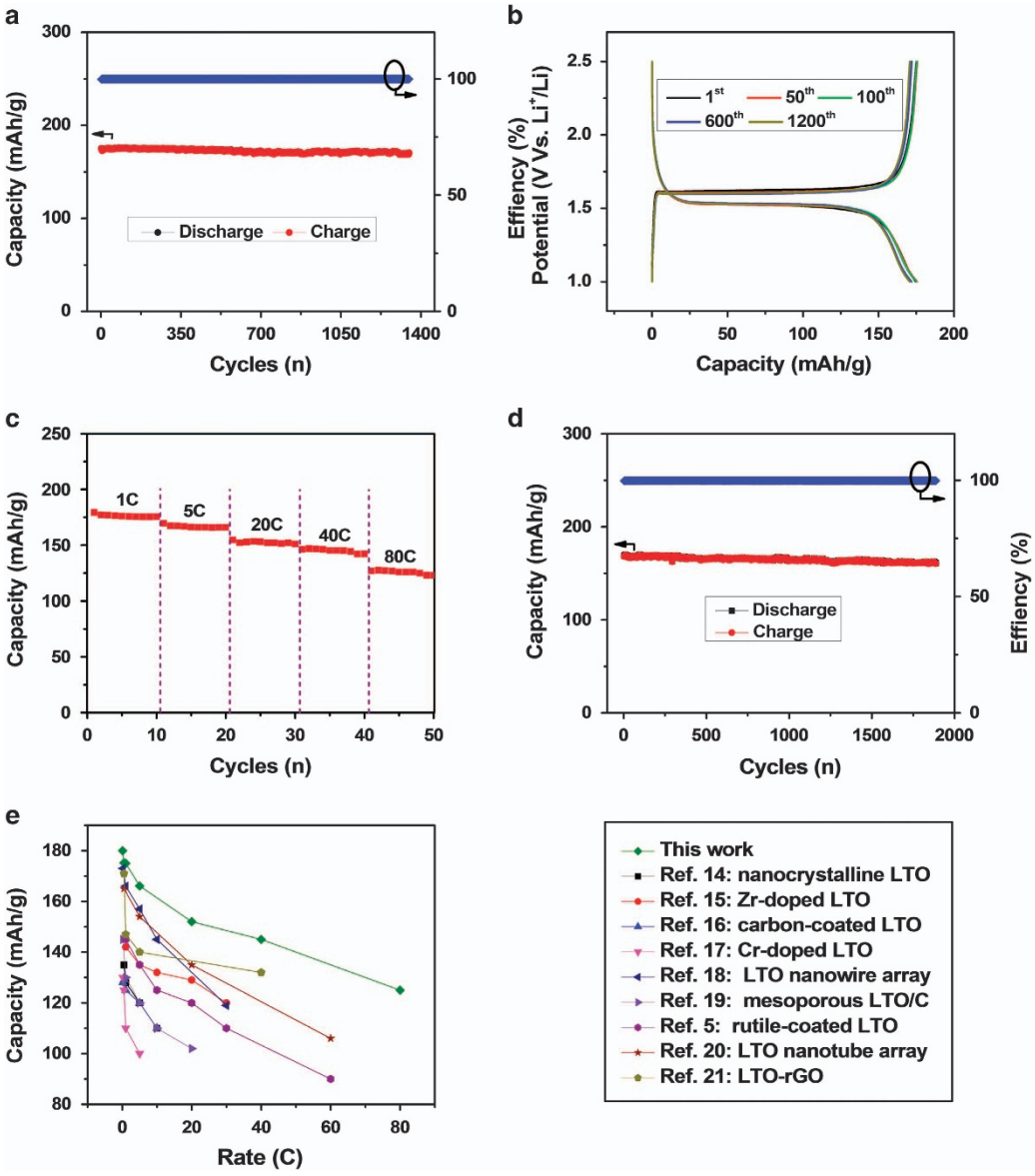

Figure 3 Electrochemical characterization of Cu/LTO scaffold: (**a**) Cycling performance and corresponding efficiency of Cu/LTO hybrids at the rate of 0.5 C. (**b**) The galvanostatic discharge/charge voltage profiles of Cu/LTO at 0.5 C in the 1st, 50th, 100th, 600th and 1200th cycles. (**c**) Comparison of the rate capabilities of Cu/LTO and LTO NPs. (**d**) The cycling performance and corresponding Coulombic efficiency of Cu/LTO at 1 C. (**e**) Comparison of the rate capability of Cu/LTO scaffolds with other recently reported LTO-based high rate electrodes. The capacities were estimated based on their total mass of electrode materials.

The ultrafast supercapacitor-like rate performance of Cu/LTO could mainly be attributed to their three-dimensional bicontinuous architectures. This structural uniqueness can enable the simultaneous minimization of the main parts of the primary resistances encountered in the charging/discharging processes (shown in Figure 1), thereby facilitating Li^+ transfer at the interface of the electrolyte and electrode and promoting Li^+ diffusion in the electrode as well as electron transport. Therefore, the ultrafast lithium storage in Cu/LTO can be perfectly realized. In addition, hydrogenation (annealing treatment of precursors in Ar/H_2) can produce Ti^{3+} sites in Cu/LTO to further improve its electronic conductivity and, thus, its rate performance.[18] As verified by X-ray photoelectron spectroscopy (XPS; Supplementary Figure S6), the two positive peaks centered at 463.3 and 457.6 eV should be attributed to the $Ti2p_{1/2}$ and $Ti2p_{3/2}$ peaks of Ti^{3+} by subtracting the normalized Ti2p spectra of Cu/LTO with LTO NPs (Supplementary Figure S6b).[18]

More importantly, the excellent high-capacity properties of Cu/LTO under both high and low rates are believed to originate from their unique structural features. Among them, the crystal plane effect has an important role.[12] On the edge of Cu/LTO NPs, there are many exposed high energy {111} facets resulting from the space confining effect of the nanosized pores. As revealed in Figure 4a, together with the FFT pattern (inset), LTO surfaces are terminated by a high density of atomic steps and kinks together with many zig-zag interfaces. For example, only a small piece of the surface (Figure 4b) is composed of eight terraces separated by atomic steps. The defects found in them may be consistent with the high surface free energy of LTO (111) compared with the (110) plane ($\gamma(110) < \gamma(111)$).[25] Generally, the

high density of atomic steps is believed to be one of the important origins of the high catalytic or electrochemical activities of small nanomaterials.[10–13] Similarly, this feature of Cu/LTO may facilitate the enhancement of the electrochemical performance of LTO.

Considering the highly exposed high-energy (111) facets and the high density of atomic steps present on the surface of Cu/LTO, its Li^+ storage mechanism is believed to be different from that of bulk LTO. Herein, the well-defined structure of Cu/LTO is visualized

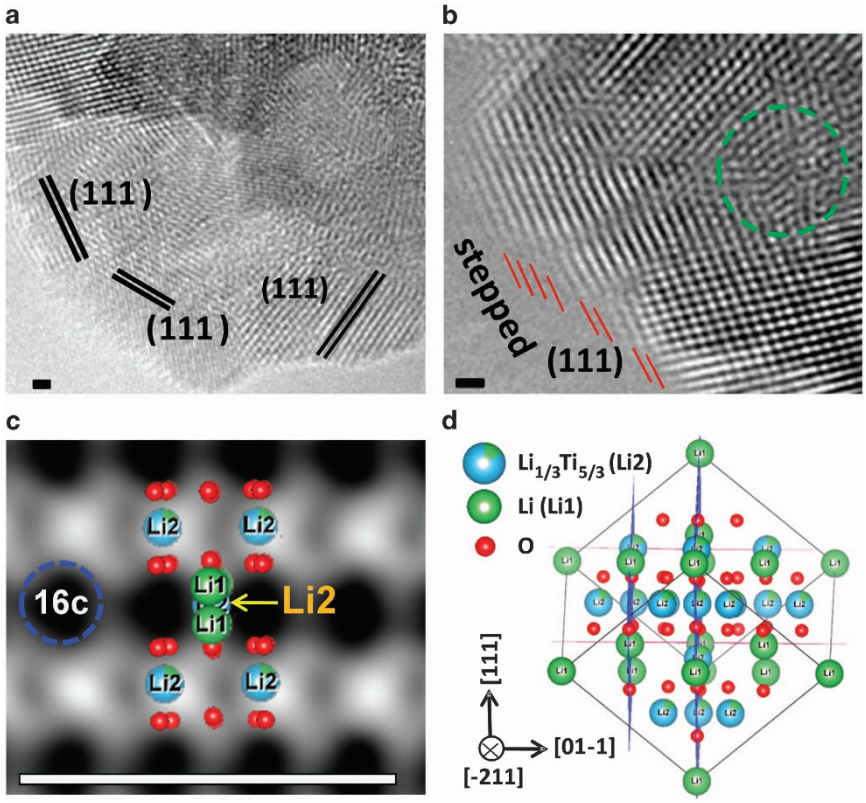

Figure 4 The detailed morphologies of the Cu/LTO edge: (**a**) HRTEM image taken of the edge area of Cu/LTO. (**b**) HRTEM image of a piece of the exposed LTO (111) planes showing a stepped surface. The green circle denotes a defect on the surface. (**c**) The enlarged (FFT inverse) image of LTO NPs taken from Cu/LTO, where the black holes denote the 16c (vacancy) sites and Li2 represents $Li_{1/3}Ti_{5/3}$. (**d**) The corresponding schematic lattice of LTO. Scale bar: 1 nm.

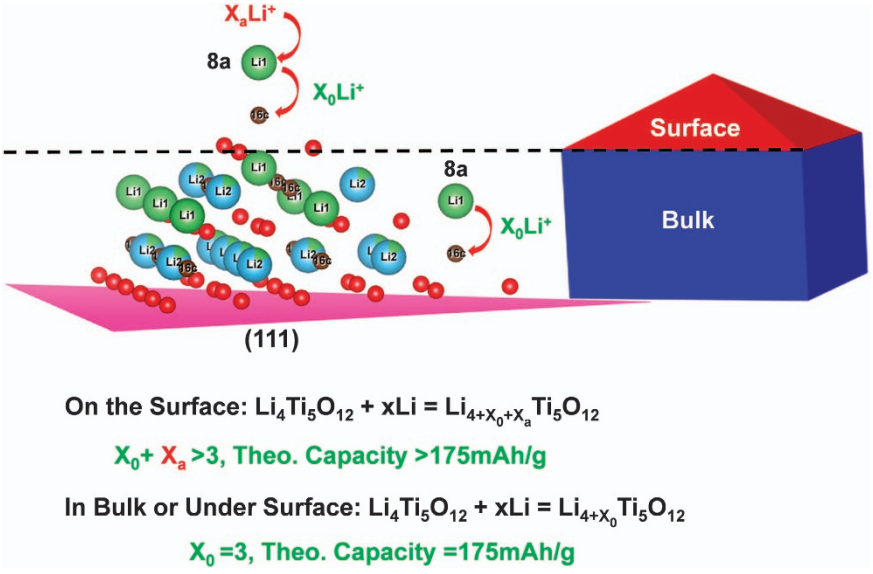

Figure 5 The unique storage mechanism of Cu/LTO: A schematic illustration of a possible storage mechanism for Cu/LTO with highly exposed (111) facets based on DFT calculations. On the surface, two types of Li ions migrate during the lithiation process; x_a represents the additional Li ions occupying vacant 8a sites, and x_0 denotes the Li ions transported from 8a to 16c sites. In the bulk or under the surface, only Li ions from 8a sites (x_0) can insert/deinsert into/from 16c sites. The theoretic capacity is thus 175 mAh g^{-1}.

directly by using high-angle annular dark-field detectors in scanning transmission electron microscopy (STEM-HAADF).[26] As shown in the enlarged (FFT inverse) image (Figure 4c), the black holes represents the vacant 16c sites, and Li1 denotes the 8a sites. Figure 4d shows the corresponding [−211] projection of the LTO structure, in which Li, O, and $[Li_{1/3}Ti_{5/3}]$ atoms/slabs are directly observed because separate columns of these atoms are aligned in this direction. Different colored balls are used to describe the different atoms or slabs.

$$[Li]_{8a}[\,]_{16c}[Ti]_{16d}\left[Li_{1/3}Ti_{2/3}\right]_{16d}[O_4]_{32e} \Leftrightarrow [\,]_{8a}[Li]_{16c}[Ti]_{16d}\left[Li_{1/3}Ti_{2/3}\right]_{16d}[O_4]_{32e} \quad (1)$$

On the basis of the density functional theory calculations illustrated in Figure 5, the exposed surface will greatly impact the capacity of the LTO. We first investigated the exact storage mechanism of bulk LTO, which could be precisely depicted as $[Li]_{8a}[\,]_{16c}[Ti]_{16d}[Li_{1/3}Ti_{2/3}]_{16d}[O_4]_{32e}$ (where a blank bracket denotes a vacancy, Equation 1). Upon lithiation, Li ions will migrate from the tetrahedral 8a to the octahedral 16c sites, and 8a will be emptied to attain the final $Li_7Ti_5O_{12}$ composition with a theoretical capacity of 175 mAh g^{-1} (Figure 5). Similar to the size effects in the $Li_{4+x}Ti_5O_{12}$ spinel,[25] the additional Li was predicted to occupy the 8a sites for LTO (111) because 16c sites in the final $Li_7Ti_5O_{12}$ composition are almost fully occupied. In fact, by adding Li to the vacant 8a sites in the (111) slabs (such that all 16c sites are occupied), the stoichiometric lithium content can be exceeded up to the composition of $Li_{8.5}Ti_5O_{12}$ before reaching a negative voltage[25] (Supplementary Figure S6) that is significantly larger than theoretical value of 175 mAh g^{-1} ($Li_7Ti_5O_{12}$); even before approaching 1 V, the final composition will be $Li_{7.75}Ti_5O_{12}$ (Supplementary Figure S7), which is slightly improved over $Li_7Ti_5O_{12}$. This result is consistent with the larger capacity found in electrochemically charged epitaxial-grown films.[13] It is noted that this is different from the case of bulk LTO, but similar to the nanosized; a higher reversible capacity ($Li_{8.5}Ti_5O_{12}$) can be achieved only as the bulk spinel $Li_{4+x}Ti_5O_{12}$ discharges down to 0.01 V, and the end composition of $Li_{7.84}Ti_5O_{12}$ can be realized when the 12 nm $Li_{4+x}Ti_5O_{12}$ discharges to 0.9 V.[25] This result suggests that increasing the amount of (111) planes on the surface of the LTO can greatly enhance the capacity. In addition, the calculated average insertion voltage of LTO (111) (to $Li_7Ti_5O_{12}$) was determined to be 1.77 V, which is higher than the 1.57 V of the bulk LTO (the experimental value is ~1.55 V). This result agrees with the observation that Cu/LTO's insertion voltage is slightly higher than that of the LTO NPs. Here we should note that only ~175 mAh g^{-1}, or a slightly enhanced capacity, is achieved for Cu/LTO. Therefore, as depicted in Figure 5, the simultaneous 8a and 16c occupation (8a +16c) mechanism may be applicable in the highly exposed (111) facets on the surface, whereas under the surface, the Cu/LTO will obey the bulk's storage rule of the occupation of 16c sites by Li ions and the emptying of 8a sites. This result further indicates that increasing the proportion of (111) facets will increase the storage capacity of LTO.

Safety is vital for the application of electrodes in LIBs. The gas-releasing of the electrode during the charge/discharge process usually leads to safety problems. A previous study[26] showed that the coexistence of two phases in the bulk LTO is believed to be responsible for the gas-releasing issues (package swelling) when LTO is used as an anode in full batteries. However, the above phenomenon is not observed in Cu/LTO (Supplementary Figure S8), which suggests that it may be a safe anode. This may be related to the protective role of the nanoporous Cu scaffolds, analogous to wearing a coat.

In summary, we have demonstrated a new 'one stone, two birds' strategy to create a bicontinuous Cu/LTO consisting of nanoporous Cu scaffolds and encapsulated LTO NPs with highly exposed (111) planes. These unique features not only provide efficient and rapid pathways for ion and electron transport but also generate additional lithium insertion sites on the surface of the LTO, thereby realizing high-rate and high-capacity lithium storage. As tested as an anode in LIBs, Cu/LTO showed superior performance, including a great than 2000 cycle lifespan and an ultrafast charging time. Notably, the ultrahigh capacity slightly larger than the theoretical value was also observed in Cu/LTO at a low current density, and density functional theory calculations and detailed characterizations revealed its unique storage mechanism (8a+16c), which differs from the transition between 8a and 16c in bulk LTO. Our findings suggest that enhancing the concentration of the high-energy plane on the electrodes' surface is another promising method to fabricate advanced electrodes for lithium storage.

CONFLICT OF INTEREST

The authors declare no conflict of interest.

ACKNOWLEDGEMENTS

This work was supported by the International Center for Young Scientists, World Premier International Research Center on Materials Nanoarchitectonics, MEXT, Japan. We greatly thank Dr Xizheng Liu at AIST, Japan for kind discussions and help.

Author contributions: XW and DL performed the experiments and testing. QL performed the density functional theory calculation. All the authors discussed the results and commented on the manuscript.

1 Pikul, J. H., Zhang, H. G., Cho, J., Braun, P. V. & King, W. P. High-power lithium ion microbatteries from interdigitated three-dimensional bicontinuous nanoporous electrodes. *Nat. Commun.* **4**, 1732 (2013).
2 Liu, N., Lu, Z., Zhao, J., McDowell, M. T., Lee, H.-W. & Cui, Y. A pomegranate-inspired nanoscale design for large-volume-change lithium battery anodes. *Nat. Nanotechnol.* **9**, 187–192 (2014).
3 Yang, S. B., Gong, Y. J., Liu, Z., Zhan, L., Hashim, D. P., Ma, L. L., Vajtai, R. & Ajayan, P. M. Bottom-up approach toward single-crystalline VO_2-graphene ribbons as cathodes for ultrafast lithium storage. *Nano Lett.* **13**, 1596 (2013).
4 Kang, B. & Ceder, G. Battery materials for ultrafast charging and discharging. *Nature* **458**, 190–193 (2009).
5 Wang, Y. -Q., Gu, L., Guo, Y.-G., Li, H., He, X.-Q., Tsukimoto, S., Ikuhara, Y. & Wan, L.-J. Rutile-TiO_2 nanocoating for a high-rate $Li_4Ti_5O_{12}$ anode of a lithium-ion battery. *J. Am. Chem. Soc.* **134**, 7874 (2012).
6 Wang, Y. G., Wang, Y. R., Hosono, E. J., Wang, K. X. & Zhou, H. S. The design of a $LiFePO_4$/Carbon nanocomposite With a core–shell structure and its synthesis by an in situ polymerization restriction method. *Angew. Chem. Int. Ed.* **47**, 7461–7465 (2008).
7 Zhang, H., Yu, X. & Braun, P. V. Three dimensional bicontinuous ultrafast charge and discharge bulk battery electrodes. *Nat. Nanotechnol.* **6**, 277–281 (2011).
8 Yu, Y., Yan, C., Gu, L., Lang, X., Tang, K., Zhang, L., Hou, Y., Wang, Z., Chen, M. W., Schmidt, O. G. & Maier, J. Three-dimensional (3D) bicontinuous Au/amorphous-Ge thin films as fast and high-capacity anodes for lithium-ion batteries. *Adv. Energy Mater.* **3**, 281–285 (2013).
9 Liu, D., Yang, Z., Wang, P., Li, F., Wang, D. & He, D. Preparation of 3D nanoporous copper-supported cuprous oxide for high-performance lithium ion battery anodes. *Nanoscale* **5**, 1917–1921 (2013).
10 Wang, X., Weng, Q., Liu, X., Wang, X., Tang, D. M., Tian, W., Zhang, C., Yi, W., Liu, D., Bando, Y. & Golberg, D. Atomistic origins of high rate capability and capacity of N-doped graphene for lithium storage. *Nano Lett.* **14**, 1164–1171 (2014).
11 Fujita, T., Guan, P., McKenna, K., Lang, X., Hirata, A., Zhang, L., Tokunaga, T., Arai, S., Yamamoto, Y., Tanaka, N., Ishikawa, Y., Asao, N., Yamamoto, Y., Erlebacher, J. & Chen, M. Atomic origins of the high catalytic activity of nanoporous gold. *Nat. Mater.* **11**, 775–780 (2012).
12 Liu, D., Wang, X., Wang, X., Tian, W., Bando, Y. & Golberg, D. Co_3O_4 nanocages with highly exposed {110} facets for high-performance lithium storage. *Sci. Rep* **3**, 2543 (2013).
13 Hirayama, M., Kim, K., Toujigamori, T., Cho, W. & Kanno, R. Epitaxial growth and electrochemical properties of $Li_4Ti_5O_{12}$ thin-film lithium battery anodes. *Dalton Trans.* **40**, 2882–2887 (2011).

14 Prakash, A. S., Manikandan, P., Ramesha, K., Sathiya, M., Tarascon, J. M. & Shukla, A. K. Solution-combustion synthesized nanocrystalline Li4Ti5O12 as high-rate performance Li-ion battery anode. *Chem. Mater.* **22**, 2857–2863 (2010).
15 Kim, J.-G., Park, M.-S., Hwang, S. M., Heo, Y.-U., Liao, T., Sun, Z., Park, J. H., Kim, K. J., Jeong, G., Kim, Y.-J., Kim, J. H. & Dou, S. X. Zr^{4+} doping in Li4Ti5O12 anode for lithium-ion batteries: open Li^+ diffusion paths through structural imperfection. *ChemSusChem* **7**, 1451–1457 (2014).
16 Li, B., Han, C., He, Y., Yang, C., Du, H. D., Yang, Q. H. & Kang, F. Y. Facile synthesis of $Li_4Ti_5O_{12}$/C composite with super rate performance. *Energy Environ. Sci.* **5**, 9595–9602 (2012).
17 Song, H., Yun, S. W., Chun, H. H., Kim, M. G., Chung, K. Y., Kim, H. S., Chod, B. W. & Kim, Y. T. Anomalous decrease in structural disorder due to charge redistribution in Cr-doped $Li_4Ti_5O_{12}$ negative-electrode materials for high-rate Li-ion batteries. *Energy Environ. Sci.* **5**, 9903–9913 (2012).
18 Shen, L., Uchaker, E., Zhang, X. & Cao, G. Hydrogenated $Li_4Ti_5O_{12}$ nanowire arrays for high rate lithium ion batteries. *Adv. Mater.* **24**, 6502 (2012).
19 Shen, L., Zhang, X. G., Uchaker, E., Yuan, C. & Cao, G. Z. $Li_4Ti_5O_{12}$ nanoparticles embedded in a mesoporous carbon matrix as a superior anode material for high rate lithium ion batteries. *Adv. Energy Mater.* **2**, 691–698 (2012).
20 Liu, J., Song, K., Aken, P. A. v., Maier, J. & Yu, Y. Self-supported $Li_4Ti_5O_{12}$–C nanotube arrays as high-rate and long-life anode materials for flexible Li-ion batteries. *Nano Lett.* **14**, 2597–2603 (2014).
21 Chen, W., Jiang, H., Hu, Y.j., Dai, Y. & Li, C. Mesoporous single crystals $Li_4Ti_5O_{12}$ grown on rGO as high-rate anode materials for lithium-ion batteries. *Chem. Commun.* **50**, 8856–8859 (2014).
22 Zhang, Q. & Li, X. Recent developments in the doped- $Li_4Ti_5O_{12}$ anode materials of lithium-ion batteries for Improving the Rate Capability. *Int. J. Electrochem. Sci.* **8**, 6449 (2013).
23 Pfanzelt, M., Kubiak, P., Fleischhammer, M. & Wohlfahrt-Mehrens., M. TiO_2 rutile—An alternative anode material for safe lithium-ion batteries. *J. Power Sources* **196**, 6815–6821 (2011).
24 Borghols, W. J. H., Wagemaker, M., Lafont, U., Kelder, E. M. & Mulder, F. M. Size effects in the $Li_4Ti_5O_{12}$ spinel. *J. Am. Chem. Soc.* **131**, 17786–17792 (2009).
25 Ganapathy, S. & Wagemaker, M. Nanosize storage properties in spinel $Li_4Ti_5O_{12}$ explained by anisotropic surface lithium insertion. *ACS Nano* **6**, 8702–8712 (2012).
26 Lu, X., Zhao, L., He, X., Xiao, R., Gu, L., Hu, Y.-S., Li, H., Wang, Z., Duan, X., Chen, L., Maier, J. & Ikuhara, Y. Lithium storage in $Li_4Ti_5O_{12}$ spinel: the full static picture from electron microscopy. *Adv. Mater.* **24**, 3233–3238 (2012).

Supplementary Information accompanies the paper on the NPG Asia Materials website (http://www.nature.com/am)